Available online at www.sciencedirect.com
SCIENCE DIRECT®
Journal of Nuclear Materials 351 (2006) 47–55
journal of nuclear materials
www.elsevier.com/locate/jnucmat

Atomic scale modelling of the primary damage state of irradiated fcc and bcc nanocrystalline metals

M. Samaras [a,*], P.M. Derlet [a], H. Van Swygenhoven [a], M. Victoria [b,c]

[a] Paul Scherrer Institute (PSI), NES/High Temperature Materials Group, NUM/ASQ, CH-5232 Villigen-PSI, Switzerland
[b] Lawrence Livermore National Laboratory, USA
[c] Polytechnic University of Madrid, Spain

Abstract

Large scale molecular dynamics computer simulations of the irradiation of nanocrystalline fcc Ni and bcc Fe show differences in defect production, with different vacancy cluster structures forming during displacement cascades. Differences in defect production also exist in comparison to their single crystal counterparts. The primary damage state after irradiation is discussed in terms of defect production as a consequence of the grain boundaries present and of the crystalline structure in order to describe the effect of these microstructural parameters.

1. Introduction

A better understanding of the life-time assessment of materials components under irradiation requires an understanding at the microscopic level of single defect damage. Modelling of their microstructure has been undertaken using Molecular Dynamics (MD) computer simulations of the displacement cascade evolution during the initial stages of radiation damage (see for example [1–3]). Such simulations have been predominantly performed in single crystal bcc Fe [4–7] and fcc Cu [3,8] with fewer simulations in fcc Ni [9].

Displacement cascades occur when energetic primary knock-on atoms (PKAs) displace atoms from their lattice sites to form vacancies and self interstitial atoms (SIAs). As the sample cools, about 80% of the Frenkel pairs produced in the collision stage of the cascade recombine. Our interest focuses on the uncombined Frenkel pairs that remain as defect damage within the sample. Their abundance, combination in clusters, mobility and absorption by sinks define the changes seen in mechanical properties of irradiated materials [10] and are therefore of great interest. To address the absorption of these defects at sinks such as grain boundaries (GBs), the samples simulated in this work are nanocrystalline (nc) structures. The presence of a high density of GBs in nc materials has been found to play a dominant role in the mechanical properties of such materials [11–13] and indicates that nc materials should have increased radiation resistance due to the large number of sink sources present in the samples [14,15], with significant reductions in defect

* Corresponding author. Tel.: +41 (0) 56 310 4184.
E-mail address: maria.samaras@psi.ch (M. Samaras).

0022-3115/$ - see front matter © 2006 Elsevier B.V. All rights reserved.
doi:10.1016/j.jnucmat.2006.02.030

production compared to their coarser grain counterparts. Indeed, ion-irradiation of nc materials has found that the defect density rapidly saturate in terms of dose [14,16,17].

In the MD timeframe, the formation and movement of SIAs has been extensively studied because of their important role in the long-term properties of irradiated materials. Single crystal displacement cascade simulations found that the SIA cluster size and fraction is larger in fcc Cu [5,8] than in bcc Fe [4–6]. The differences in the glissile to sessile fraction of SIA clusters formed in the different structures during irradiation [18] is postulated as the possible cause for the qualitatively differences in SIA cluster size [19]. Indeed, all bcc Fe SIA clusters are believed to be glissile leading to little clustering [19] which contrasts the large number of sessile SIA clusters found in fcc [19]. The defect configurations in which small Fe clusters exist and move have been carefully identified with ab initio calculations [20]. The mobility of glissile SIA clusters has been classified as 1D/3D or 1D (for large clusters) motion along close packed planes, with a more precise description given in terms of Brownian motion [21]. The presence of GBs complicates such SIA movement, with larger SIA clusters, seen to move 1D in single crystals, observed moving 1D/3D in nc Ni [22] as a result of the pressure gradients present in the GBs [23]. This movement leads to their absorption at pre-existing defects [22,24], surfaces [25–28] and within GBs [29–31] at GB dislocations and triple junctions [31]. Therefore, understanding SIA production and mobility is vital in understanding the changes in the microstructural behaviour of materials under irradiation.

The formation of SIA defects during a displacement cascade indicates the presence of vacancies. Vacancy defect formation has been found to depend on the crystal structure with irradiation experiments in Cu and Ni producing stacking fault tetrahedra (SFTs) with sizes of the order of 2–3 nm [14,32–34] as the main vacancy defect, whereas in Fe no defects were observed [35] until positron annihilation experiments revealed the existence of micro-voids [36]. Such results are reproduced in fcc simulations with SFT like vacancy clusters forming in single crystal Cu [37] and nc Ni [38] because of a greater ease to cluster than bcc Fe [7,39,40] where (like other bcc metals [41]) small isolated defects were produced [5,7]. These differences are accounted for by the various clustering efficiencies of the crystalline structures as well as the mobility of SIAs and therefore their ability to annihilate with forming vacancies.

In this work, we address the role of the GB as a function of the crystalline structure by comparing the behaviour of damage production in nc fcc Ni and bcc Fe metals. The structure, density and thickness of GBs present in the samples is compared in order to set up a precedence on which to perform cascade simulations. Results of displacement cascade simulations are presented, compared and discussed, with an emphasis on the size of the cascades formed, number and types of defects produced as well as the role of GBs during these cascades.

2. Method

Samples containing 1.2 million (fcc) and 1.4 million (bcc) atoms are simulated using the Voronoi [42] construction to obtain a fully three dimensional grain structure containing 15 grains with 12 nm average sized grain diameters. In the case of Ni, the structure of these GBs has been extensively investigated [12,13,43]. To obtain an equilibrated structure, the samples are relaxed using molecular statics and then MD at 300 K for 150 ps.

The nc fcc Ni sample implements the Cleri and Rosato second moment tight binding potential [44] with modifications for the short range atomic interactions following Ziegler et al. [45]. The Ackland potential [46] is used in the bcc Fe simulations. It is important to note that empirical potential approaches are of limited value as they do not take into account the significance of the magnetism present which plays a fundamental role in determining interatomic interactions. It is known that the primary damage produced as a result of a displacement cascade is sensitive to the potential used with various potentials producing very different results. The SIA stability predicted is one such example; the $\langle 1\,1\,0\rangle$ dumbbell is the most stable configuration seen experimentally [47] and is predicted by the Ackland potential. In this study, the Ackland potential has been implemented in order to make comparison to the large number of simulations that exist with this potential. Better potentials have been developed [48], however, the general limitation met by all these potentials in ignoring the role of magnetism signifies that although the Ackland potential is less accurate, it is still a valid empirical potential which may be used to study bcc Fe.

The inclusion of the electron–phonon interaction which can be included as a damping term in the equations of motions [49], shortens the lifetime of the thermal spike during the displacement cascade [49,50]. The stronger the electron–phonon interaction the higher the number of defects produced and the larger the vacancy clustering fraction, however the size distribution of SIA has been found not to change [50]. As the electron–phonon interaction can only be included as a varying damping parameter, in this study it has not been included so that comparisons can be made to early results produced with the Ackland potential.

Insight into the GB structure and SIA movement has been obtained by studying the local pressure present in the relaxed samples [51,23]. The local pressure is calculated as the average pressure within a 4 Å volume element centred on each atom. Time averaging of approximately 1 ps is done in order to average over thermal vibrations. A colour scheme is then allocated, for the range −1.2 GPa (purple) to 2.8 GPa (red), where a positive value represents compression and a negative value represents tension. We note that due to the non-volume conserving nature of the atomic volumes for which the pressure is calculated, the local pressures do not sum up to the global stress of the systems. For further details refer to [23].

The displacement cascade simulations are undertaken at room temperature with periodic boundary conditions using MD. Heat is extracted from the sample via velocity rescaling of a thin outer shell of atoms at the periphery of the box. The cascade is initiated by choosing a primary knock-on atom (PKA) of 5–20 keV which receives the entire energy and a direction. As the sample cools, the evolution of the displacement cascade is monitored and results are reported below.

3. Results

In order to make comparisons of displacement cascades in the two structures, nc fcc Ni and bcc Fe, the differences and similarities present in the relaxed samples are first described. The density of the nc materials compared to their bulk counterparts, which expresses the free volume present in GBs in the sample, is 97.3% in nc fcc Ni and 99.25% in nc bcc Fe respectively. As seen in studies of nc fcc Ni [12,13,43], the bcc Fe GB structure is found to be made up of structurally ordered regions which repeat themselves to makeup the GB. Since atoms situated at the GB have a higher energy than atoms in fcc/bcc lattice positions, an energy cutoff criterion can be used to look at the number of atoms in the GBs. The cutoff is taken so that the GBs have a 3–4 atom width, which is the thickness seen from the crystalline order definition of GBs in Ni [43]. In the Ni sample 5.4% of atoms and in the Fe sample 7.5% of atoms are in this high energy range and are found to be situated almost entirely in GB positions.

The pressure gradients in the relaxed GB structure [51] have been found to play a significant role in determining the SIA cluster paths to the GB in fcc Ni [23] and are therefore shown for nc bcc Fe (Fig. 1(a)) and nc fcc Ni (Fig. 1(b)). The general trends occurring as a result of the pressure gradients present in nc samples are now discussed. Fig. 1(a) shows that in Fe, regions of oscillating pressure encompass the interphase regions and comprise of alternating regions of high compression (red atoms) and high tension (purple atoms) which sum to a net tensile pressure. The grain itself has very little pressure indicated by the close to zero pressure colours of green to light blue. Fig. 1(b), picturing fcc Ni pressure gradients, shows similar local pressure characteristics [23]. The figures indicate that both nc samples are similarly constituted of pressure gradients which encompass the interphase regions and which are present as a consequence of the nc structure of the sample. Using the setting of a GB structure, comparisons are made between nc fcc Ni and bcc Fe to determine the influence of the GB and crystalline structure on displacement cascades.

4. Displacement cascade simulations

The maximum cascade volume as a result of 5 keV PKAs, in samples containing 5.8 (Ni) and 7.3 (Fe) million atoms are shown in Fig. 2 from two different views. The irradiated grains of 18 nm nc bcc Fe (green) and 20 nm nc fcc Ni (pink) are also visualised in like colours in order to show the proximity and size of the cascade compared with the grain it irradiates. The maximum cascade volumes are defined as the volume encompassing the largest region of higher energy atoms (using the same criterion as described above for GBs) during the displacement cascade. Superimposing the cascades over each other reveals that they are equivalent in size, and indicates that the crystalline structure of the material does not influence the size of displacement cascades introduced into the samples.

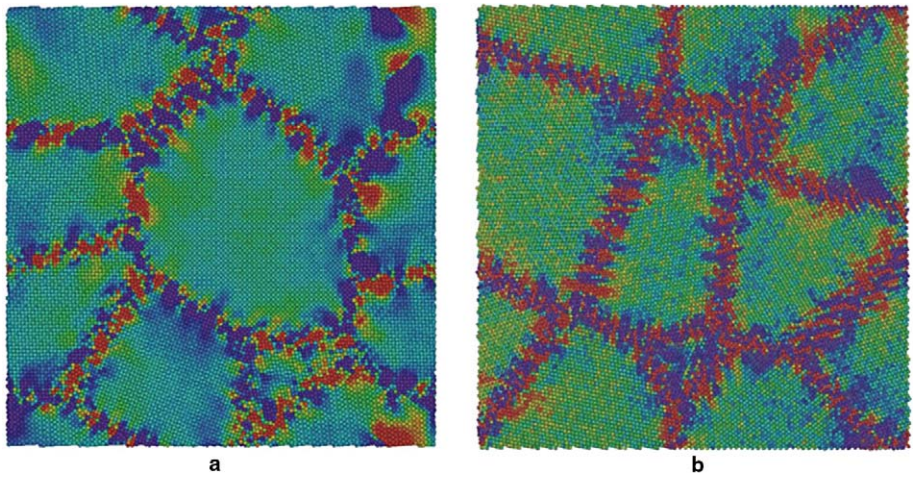

Fig. 1. Pressure present in the relaxed samples in (a) bcc Fe and (b) fcc Ni. The GBs are made up of adjacent regions of high tensile and high compressive pressure.

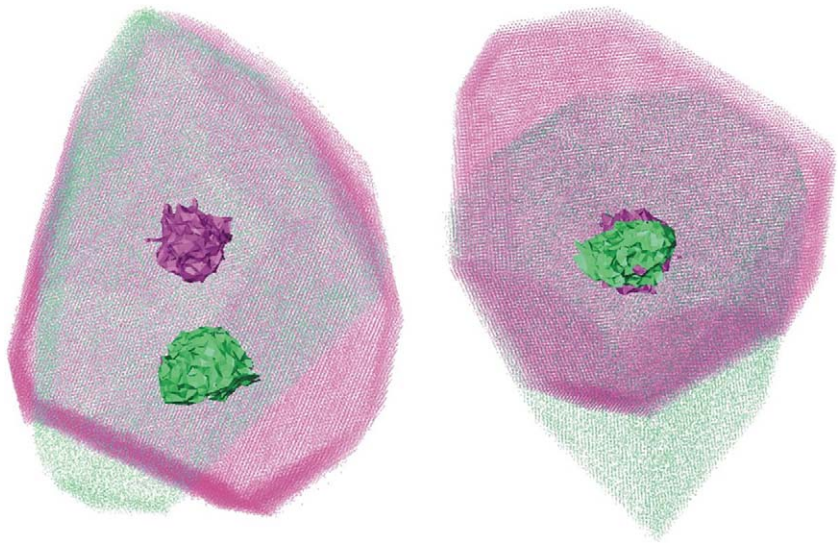

Fig. 2. Comparison of maximum cascade volume of 18 nm bcc Fe (pale grey/green online) and 20 nm fcc Ni (dark grey/pink online) in two different orientations with irradiated grains shown as a reference in respective colours.

Figs. 3 and 4 are the average statistics obtained from simulation of four 5 keV, five 10 keV and five 20 keV PKA simulations. The comparisons to single crystal results are from one 5 keV, one 10 keV and two 20 keV PKA simulations. Fig. 3 shows that the number of defects produced from the 5 keV simulations are similar in both the single crystal (black) and the nc (grey) samples. The numbers indicate that the number of vacancies formed in both samples are about the same. The 10 keV and 20 keV results reveal that simulations in the nc sample produce about double the number of vacancies. Simulations in nc fcc Ni [38] similarly show that the number of vacancies is much larger in the nc than in the single crystal. In order to properly assess the 5 keV simulations, more simulations need to be done with a varying distance to the GB. The 5 keV results indicate that at the distance (between 1.3 and 2.2 nm from the nearest GB), the GBs do not have enough strength to attract the SIAs during the thermal spike, but instead absorb the SIAs after they have formed clusters within the grain. This indicates that there seems to be a distance dependence of the cascade to interact directly with the

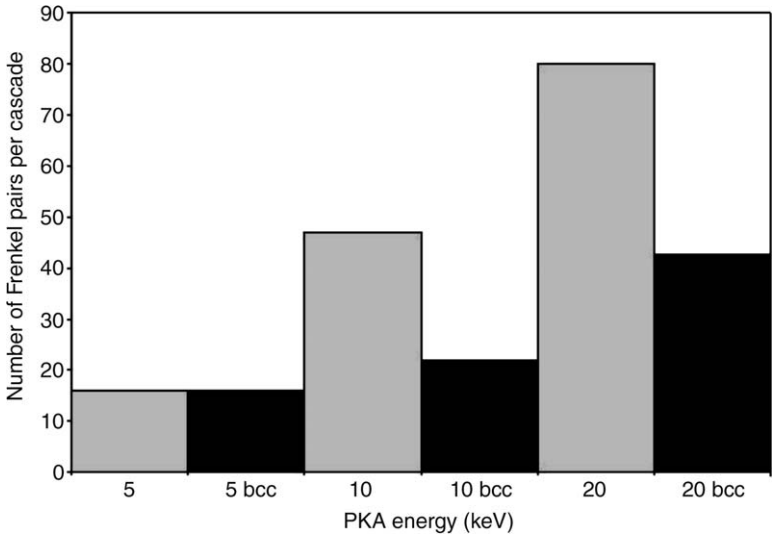

Fig. 3. Average of the total Frenkel pairs produced during displacement cascades as a function of PKA energy.

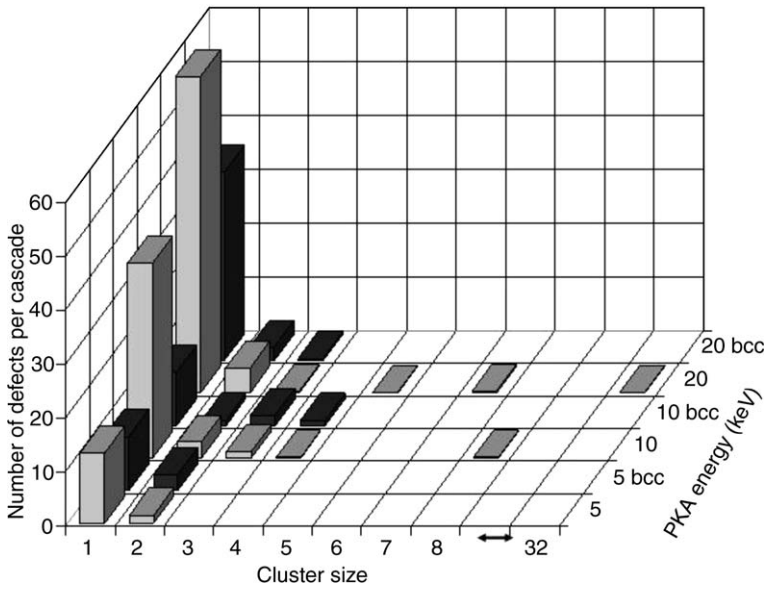

Fig. 4. The average of vacancy defect clusters produced in single and nc bcc Fe simulation cascade as a function of PKA energy.

GB during the ballistic phase with less Frenkel pairs reuniting due to the movement of SIAs to the nearby GBs.

Fig. 4 shows the vacancy cluster size distribution at the end of the cascade as a function of the recoil energy for the nc bcc Fe sample (grey) and is compared to single crystal Fe results (black) obtained using the same potential. The single crystal simulations show that a small amount of clustering is produced in the bcc Fe matrix in single crystal simulations, with clusters containing a maximum of four vacancies. This is in agreement with other single crystal bcc Fe simulations which obtained a maximum of five vacancies in clusters in the 5–20 keV range at 100 K [52]. In contrast, the nc sample produced larger clusters, including the formation of a cluster containing 35 vacancies according to the nearest neighbour criterion. If vacancies sitting in next to nearest neighbour positions were also included, the vacancy cluster would be larger. Such

'nascent vacancy clusters' [53] are expected to coalesce into one larger cluster over a timeframe beyond MD [53]. In 20 keV PKA simulations, the cascade often splits into subcascades or is situated with GBs and triple junctions in the cascade core region, resulting in the cascade overflowing into neighbouring grains resulting in up to three grains being irradiated. In nc fcc Ni, at this energy, overflow of the displacement cascade into neighbouring grains was not so frequently seen. Whether the structure affects the ability of the GB to retain a cascade in one grain or whether the cascade overflow seen in bcc nc Fe so far is due to subcascading is still an open question.

Fig. 5(a) describes the typical movement of SIAs formed during displacement cascade simulations in nc bcc Fe. The black lines show the movement of atoms during a 5 keV PKA cascade, superimposed onto the local pressure present in the relaxed sample. The lines show the presence of both 1D and 1D/3D movement of SIAs to the nearby GB structure, which enables them to reach the GB at regions of high tensile pressure (purple spheres). The termination of the lines indicate where the SIA clusters stop their motion, which occurs as a result of their accommodation in the GB structures and their annihilation with free volume existing therein. In our nc bcc Fe displacement cascade simulations, all SIAs leave the irradiated grain and are absorbed by the GB within the MD simulation timeframe. A similar high mobility of Fe SIAs has also been reported in single crystal simulations (with all bcc Fe SIA clusters thought to be glissile [19]), in surface simulations which absorb all SIAs [54] and experimentally where no damage is seen [35].

Almost all SIAs are absorbed by the GB during the simulations; the majority being absorbed during the ballistic phase in the 10 and 20 keV simulations. The largest SIA clusters found in the 5 keV, 10 keV and 20 keV simulations contain five, four and three SIAs respectively. In comparison, the largest SIA clusters in our single crystal results contain seven, six and eight SIAs in 5 keV, 10 keV and 20 keV PKAs respectively, which compares well to previous single crystal studies done at 100 K where a maximum of six, seven and seven SIAs in clusters were obtained respectively for the three PKA energies [52]. The maximum SIA cluster size of the 5 keV results is similar in both the single crystal and nc. However, the 10 and 20 keV maximum cluster size is much smaller in the nc simulations which seems to be due to the close proximity of GBs which often absorb the SIAs during the ballistic phase and before they have an opportunity to interact with one another to form larger SIA clusters.

Using the same colour scheme as in Fig. 5(a), a section of the pressure gradients present in the relaxed nc fcc Ni sample are shown in Fig. 5(b). The black lines reveal that a large number of SIAs move to the GB and triple junction region composed of high tensile pressure (purple) situated in the bottom left corner. One mono-SIA (to the right) initially moves parallel to the GB in order to avoid the region of high compressive pressure which separates it from the GB. Once it has reached a region of near zero pressure, it stops, and sensing a region of

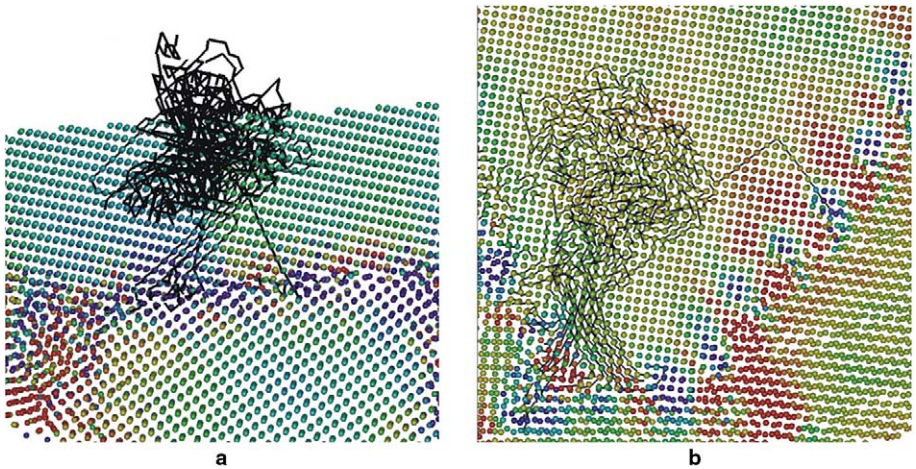

Fig. 5. Black lines indicate the movement of atoms during the displacement cascade in (a) bcc Fe and (b) fcc Ni on a backdrop of the pressure present in the relaxed sample. The interstitials move to the nearby GB structure at high tensile pressure.

high tensile pressure in the distance, changes direction to move to the GB. Such 1D/3D motion was also seen for larger SIA clusters containing up to eight SIAs [23]. In our nc fcc Ni, almost all SIA clusters are glissile with the GB inducing both small and large SIA clusters to move 1D/3D under the pressure gradients present. Similar SIA mobility, which leads to the exodus of SIAs from samples to sinks, has been seen in fcc surface simulations [28], in nc Ni [15,23,31] and in nc fcc metal experiments [14,16,17] where only vacancy defect structures are observable. These results contrast the sessile nature attributed to a larger fraction of SIA clusters in fcc Cu single crystal simulations [19].

The differences seen in the mobility of single crystal SIA clusters of fcc and bcc materials is proposed to be due to the differences in close packed directions of the structures [3]. In the nc materials, all SIAs in bcc Fe and almost all SIAs in fcc Ni are seen to move to sinks (GBs) within the simulation timeframe, such that a comparison of their mobility is not an issue. Indeed, the role of the crystal structure in determining SIA mobility and clustering has been questioned because of the influence of the stacking fault energy of the various metals with SIA mobility differences occurring between Ni and Cu fcc metals [19] and between Fe and Zr bcc metals [3] resulting in a hypothesis that clustering could instead be a metal dependent phenomena [3].

In both structures, the removal of SIAs from the grain to the surrounding GBs leaves the irradiated grain with vacancy dominated defects. In single crystal displacement cascade simulations of bcc Fe, we obtain small vacancy clusters containing four or less vacancies at the various PKA energies similar to results previously seen [5,7]. This small amount of vacancy clustering is also seen in nc bcc Fe simulations when the cascade core is not in close proximity to a GB. When, however, a large cascade, for example a 20 keV PKA, is introduced in the close proximity of a GB, the production and consequent removal of a large number of SIAs leads to a larger number of vacancies in the grain as shown in Fig. 6. Fig. 6(a) shows a section of the relaxed 12 nm grained sample (the colour of the atoms having no significance). The same section of the sample, at the end of the 20 keV PKA cascade, is presented in Fig. 6(b). The GB in these figures, is discernible at the point where the atoms change orientation. Let us refer to the left grain, which contains the displacement cascade, as grain 1, and the right grain as grain 2. In the relaxed sample, Fig. 6(a), grain 2 has nine vertical rows, which we number from right to left. After irradiation, Fig. 6(b) shows that the ninth row has lengthened and that a tenth row now exists because of the GB acting as a sink and attracting SIAs. Once the SIAs have reached the GB, they move into positions which are aligned with atoms

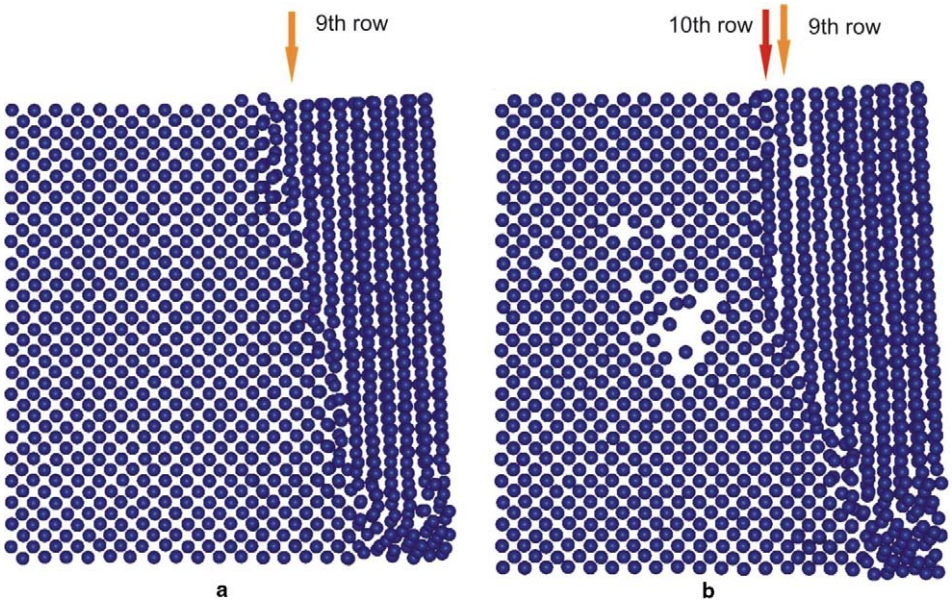

Fig. 6. (a) Section of the relaxed bcc Fe sample with GB. (b) Same section after a 20 keV PKA displacement cascade, with large and small vacancy defect clusters present.

which have a grain 2 orientation. This results in GB migration due to the influx of SIAs formed during the displacement cascade. Similar local GB migration has also been observed in nc fcc Ni displacement cascades [38]. In experiment, similar processes occur during irradiation, with the climb of dislocations occurring as a consequence of void formation [55].

In Fig. 6(b), the area of missing atoms signifies a large vacancy cluster containing 35 vacancies, with many nearby mono- and di-vacancies. Larger vacancy defect clusters have also been seen near free surface simulations due to the loss of SIAs to the surface [54] which contrasts the lack of clustering reported in single crystal simulations. Many mono vacancy clusters are also present at the end of the nc bcc Fe displacement cascade, a few of which are visible in Fig. 6(b) in the near proximity of the larger vacancy cluster. Such vacancy site correlations [56] and loose vacancy conglomerations in second to fourth nearest neighbour configurations [57] have also been seen in single crystal Fe simulations, clearly indicating that the GB's presence which attracts SIAs influences single vacancy and the number and size of vacancy clusters formed. It must be noted that within the time frame of these MD simulations, vacancy clusters are not mobile, however they are expected to move with time to be absorbed by GBs or with subsequent structural reorganisation form larger clusters.

In comparison, in nc fcc Ni displacement cascades of 10 keV PKA energy and higher, truncated stacking SFTs, of up to 3.4 nm in size, are observed [38]. The large size of these truncated SFTs has been shown to be due to the integral role of the GB during the displacement cascade which acts as a sink and removes SIA atoms from the grain so that they are unable to recombine with vacancies [15,38] and has experimentally been seen in irradiate Ni composed of 100 μm [34] and nc [14] grains, with a mean size of 2.5 nm. The formation of SFT structures in fcc crystals differs from the vacancy defects formed in bcc Fe where no SFTs are observed. This is believed to be due to the high stacking fault energy of bcc Fe which makes it unlikely to produce stacking faults and therefore vacancy clusters cannot collapse into SFT type structures [35]. Further evidence of crystalline structure influence during irradiation damage defect production is apparent in the defect density in bcc metals which is much lower than in fcc metals [32,33,39,58], with two orders of magnitude higher dose necessary in Fe to produce the same defect damage as in Ni [59]. Clearly, the structure and size of vacancy clusters formed are quite different in the two materials and is dependent not only on their crystal structure but also on the presence of GBs acting as effective sinks for SIAs.

5. Conclusion

The structure of nc samples constructed with fcc and bcc crystallinity have been compared in order to deduce the role of the GB and the crystal structure on damage production during irradiation in the search for suitable material components for irradiation. Comparison of the relaxed nc samples reveals that regardless of the crystal structure, the GBs have similar thicknesses within the relaxation timescale of the simulation and the interphase regions are composed of alternating regions of high compressive and high tensile pressure. Cascade evolution is similar in both nc metals with cascades encompassing similar volumes and producing Frenkel pairs which do not recombine but remain as damage defects within the sample. SIAs are seen to be extremely mobile and move to the GB, leaving the interior of the grain with only vacancy defects remaining. The glissile behaviour is expected of bcc Fe SIAs but is surprising for fcc Ni SIAs where a larger number of sessile SIA clusters were seen in single crystal simulations. The SIA clusters are attracted to regions of high tensile pressure and move 1D/3D to reach the GB and annihilate with free volume therein. The GB is found to be flexible and migrate to accommodate incoming SIAs. Therefore the GB is found to play a significant role in damage production during displacement cascade resulting in a larger number of vacancy defects than their single crystal counterpart. The formation of vacancy clusters, however, is sensitive to the crystalline structure of the irradiated material with stacking fault tetrahedra being produced in nc fcc Ni samples whereas large vacancy structures are produced in nc bcc Fe. The formation of much larger vacancy clusters, indicates the relevance of the inclusion of the GB due to the exodus of a much large number of SIAs which are not produced within the single crystal simulations.

Acknowledgement

Present results were obtained as part of the EFDA Modeling of Fusion Materials Subtask TW4-TTMS 007.

References

[1] D.J. Bacon, T. Diaz de la Rubia, J. Nucl. Mater. 216 (1994) 275.
[2] T. Diaz de la Rubia, Ann. Rev. Mater. Sci. 26 (1996) 213.
[3] D.J. Bacon, F. Gao, Yu. N. Osetsky, J. Nucl. Mater. 276 (2000) 65.
[4] A.F. Calder, D.J. Bacon, J. Nucl. Mater. 207 (1993) 22.
[5] W.J. Pythian, R.E. Stoller, A.J.E. Foreman, A.F. Calder, D.J. Bacon, J. Nucl. Mater. 223 (1995) 245.
[6] R.E. Stoller, G.R. Odette, B.D. Wirth, J. Nucl. Mater. 251 (1997) 49.
[7] N. Soneda, T. Diaz de la Rubia, Philos. Mag. A78 (1998) 995.
[8] T. Diaz de la Rubia, M.W. Guinan, Phys. Lett. 66 (1991) 2766.
[9] A. Almazouzi, M.-J. Caturla, T. Diaz de la Rubia, M. Victoria, Mater. Res. Soc. Symp. Proc. 540 (1999) 685.
[10] M. Victoria, N. Baluc, C. Bailat, Y. Dai, M.I. Luppo, R. Schaeblin, B.N. Singh, J. Nucl. Mater. 276 (2000) 114.
[11] C.C. Koch, D.G. Morris, K. Lu, A. Inoue, Mater. Res. Soc. Bull. 24 (1999) 54.
[12] H. Van Swygenhoven, Science 296 (2002) 66.
[13] H. Van Swygenhoven, P.M. Derlet, Phys. Rev. B 64 (2001) 224105.
[14] N. Nita, R. Schaeblin, M. Victoria, J. Nucl. Mater. 329–333 (2004) 953.
[15] M. Samaras, P.D. Derlet, H. Van Swygenhoven, M. Victoria, Phys. Rev. Lett. 88 (2002) 125505.
[16] M. Rose, A.G. Balogh, H. Hahn, Nucl. Instr. and Meth. B 127 & 128 (1997) 119.
[17] Y. Chimi, A. Iwase, N. Ishikawa, M. Kobiyama, T. Inami, S. Okuda, J. Nucl. Mater. 297 (2001) 355.
[18] B.N. Singh, J.H. Evans, J. Nucl. Mater. 226 (1995) 277.
[19] Yu. N. Osetsky, A. Serra, B.N. Singh, S.I. Golubov, Philos. Mag. A80 (2000) 2131.
[20] C.-C. Fu, F. Willaime, Phys. Rev. Lett. 92 (2004) 175503.
[21] S. Dudarev, Phys. Rev. B 65 (2002) 224105.
[22] M. Samaras, P.D. Derlet, H. Van Swygenhoven, M. Victoria, J. Nucl. Mater. 323 (2003) 213.
[23] M. Samaras, P.D. Derlet, H. Van Swygenhoven, M. Victoria, Phys. Rev. B 68 (2003) 224111.
[24] C.A. English, W.J. Phythian, A.J.E. Foreman, J. Nucl. Mater. 174 (1990) 135.
[25] M. Ghaly, R.S. Averback, Phys. Rev. Lett. 72 (1994) 364.
[26] R.S. Averback, M. Ghaly, H. Zhu, Radiat. Eff. Def. Sol. 130 & 131 (1994) 211.
[27] R.E. Stoller, J. Nucl. Mater. 307–311 (2002) 935.
[28] K. Nordlund, F. Gao, Appl. Phys. Lett. 74 (1999) 2720.
[29] K. Sugio, Y. Shimomura, T. Diaz de la Rubia, J. Phys. Soc. Jpn. 67 (1998) 882.
[30] F.J. Perez-Perez, R. Smith, Nucl. Instrum. and Meth. B 180 (2001) 332.
[31] M. Samaras, P.D. Derlet, H. Van Swygenhoven, M. Victoria, Philos. Mag. 83 (2003) 3599.
[32] Y. Dai, M. Victoria, Mater. Res. Soc. Symp. Proc. 439 (1997) 319.
[33] B.N. Singh, S.J. Zinkle, J. Nucl. Mater. 206 (1993) 212.
[34] S.J. Zinkle, L.L. Snead, J. Nucl. Mater. 225 (1995) 123.
[35] C.A. English, J. Nucl. Mater 108 & 109 (1982) 104.
[36] M. Eldrup, B.N. Singh, J. Nucl. Mater. 276 (2000) 269.
[37] Yu. N. Osetsky, D.J. Bacon, Nucl. Instrum. and Meth. B 180 (2001) 85.
[38] M. Samaras, P.D. Derlet, H. Van Swygenhoven, M. Victoria, Nucl. Instrum. and Meth. B 202 (2002) 51.
[39] M.-J. Caturla, N. Soneda, E. Alonso, B.D. Wirth, T. Diaz de la Rubia, J.M. Perlado, J. Nucl. Mater. 276 (2000) 13.
[40] Yu. N. Osetsky, D.J. Bacon, A. Serra, B.N. Singh, S.I. Golubov, Philos. Mag. 83 (2003) 61.
[41] K. Morishita, T. Diaz de la Rubia, Ion Sol. Inter. Mat. Mod. Proc. Symp. (1996) 39.
[42] G.Z. Voronoi, J. Reine, Angew. Math. 1 (34) (1908) 199.
[43] H. Van Swygenhoven, D. Farkas, A. Caro, Phys. Rev. B 62 (2000) 831.
[44] F. Cleri, V. Rosato, Phys. Rev. B 48 (1993) 22.
[45] J. Ziegler, J.P. Biersack, U. Littmark, The Stopping Range of Ions in Solids, Pergamon, New York, 1987.
[46] G.J. Ackland, D.J. Bacon, A.F. Calder, T. Harry, Phil. Mag. A 75 (1997) 713.
[47] H. Maeta, F. Ono, T.J. Kittaka, J. Phys. Soc. Jap. 53 (1984) 4353.
[48] M.I. Mendelev, S. Han, D.J. Srolovitz, G.J. Ackland, D.Y. Sun, M. Asta, Philos. Mag. A 83 (2003) 3977.
[49] A. Caro, M. Allurralde, S. Pronnecke, M. Victoria, Radiat. Eff. Def. Solids 129 (1994) 105.
[50] F. Gao, D.J. Bacon, P.E.J. Flewitt, T.A. Lewis, Model. Simul. Mater. Sci. Eng. 6 (1998) 543.
[51] A. Hasnaoui, H. Van Swygenhoven, P.M. Derlet, Acta Mater. 50 (2002) 3927.
[52] D.J. Bacon, F. Gao, Yu. N. Osetsky, J. Nucl. Mater. 276 (2000) 1.
[53] R.E. Stoller, J. Nucl. Mater. 276 (2000) 22.
[54] R.E. Stoller, S.G. Guiriec, J. Nucl. Mater. 329–333 (2004) 1238.
[55] K. Kitajima, K. Futagami, E. Kuramoto, J. Nucl. Mater. 85 & 86 (1979) 725.
[56] R. Stoller, Mater. Res. Soc. Symp Proc 540 (1999) 679.
[57] V.G. Kapinos, Yu. N. Osetsky, P.A. Platonov, J. Nucl. Mater. 173 (1990) 229.
[58] M.L. Jenkins, M.A. Kirk, W.J. Pythian, J. Nucl. Mater. 205 (1993) 212.
[59] N. Baluc, C. Bailat, Y. Dai, M.I. Luppo, R. Schaublin, M. Victoria, Mat. Res. Symp. Proc. 540 (1999) 539.